Chemical Engineering Journal 170 (2011) 7–13

Contents lists available at ScienceDirect

Chemical Engineering Journal

journal homepage: www.elsevier.com/locate/cej

Photovoltaic solar electro-oxidation (PSEO) process for wastewater treatment

Enrique Alvarez-Guerra*, Antonio Dominguez-Ramos, Angel Irabien

Departamento de Ingeniería Química y Química Inorgánica, Universidad de Cantabria, Avenida de los Castros s/n, 39005 Santander, Cantabria, Spain

ARTICLE INFO

Article history:
Received 26 November 2010
Received in revised form 14 February 2011
Accepted 15 February 2011

Keywords:
Electrochemical oxidation
Photovoltaic solar energy
Wastewater treatment
Modeling

ABSTRACT

Electro-oxidation with boron-doped diamond (BDD) electrodes has been demonstrated as an effective technology that achieves the complete mineralization of very different types of wastewater pollutants. Its main drawback is the high primary energy demand. Direct connection of photovoltaic (PV) modules to the electrochemical reactor is carried out to reduce the non-renewable primary energy consumption of the technology. The aim of this work is to model the so-called photovoltaic solar electro-oxidation (PSEO) process. For this purpose, experiments were performed with different wastewaters (urban and synthetic) at different scales (laboratory and pilot plant). A first order kinetic respecting total organic carbon (TOC) for the mineralization rate is concluded. PV modules performance is described in terms of a linear relationship between the current generated and the solar irradiance. Moreover, the definition of two efficiencies that describe the process performance is possible using model equations: current efficiency, η_c, and energy conversion efficiency, η_e.

1. Introduction

Electrochemical oxidation or electro-oxidation (EO) is the most popular electrochemical procedure for removing organic pollutants from wastewaters [1]. This technology is characterized by simple equipment, easy operation, versatility and its environmental compatibility since it does not require the addition of chemicals [2]. Among the wide variety of available electrodes, boron-doped diamond (BDD) thin-films electrodes stand out because of their useful properties, such as an inert surface with low adsorption properties and a strong tendency to resist deactivation, high resistance to corrosion, high thermal stability, hardness, good electrical conductivity or, especially, an extremely wide potential in aqueous and non-aqueous electrolytes [3,4]. This technology has been demonstrated effective to achieve the complete mineralization of the pollutants contained in wastewater of very different nature, both urban and synthetic. The efficiency of the electrochemical oxidation with BDD electrodes is very high, being limited by the transport of pollutants to the anodic surface [5]. Moreover, EO with BDD electrodes can compete satisfactorily with Fenton oxidation in the treatment of several wastewaters in terms of operation and investment costs [6]. Nevertheless, PSEO process does not substitute biological treatments since both have different areas of application. Biological treatments are not suitable for effluents which contains biorefractory compounds [2] or for applications with low flowrates (less than 25 $m^3\,h^{-1}$) [7]. In these applications, PSEO constitutes an effective and environmentally friendly wastewater treatment. PSEO process is not technically limited to biorefractory and biodegradable compounds.

On the other hand, the main disadvantage of this technology is the high energy demand, with the consequent both environmental and economic impacts [8,9]. For this reason, some examples of recent research studies in which electrochemical reactors are supplied directly by photovoltaic (PV) energy can be found in the literature [10–13], demonstrating the technical feasibility of the technology. Besides the CO_2-eq. emission reduction associated to the use of a renewable source of energy like the solar photovoltaic energy, direct connection of the modules to the reactor avoids employing energy storage systems (e.g. lead acid batteries). No need of using batteries means that the process is operated with higher efficiencies in an easier way (i.e. the control of the state of charge is not necessary), a reduction in the equipment and maintenance costs is achieved, and the environmental impact of battery production is avoided [14,15].

The aim of this work is the analysis and modeling of the process called PSEO, photovoltaic solar powered electrochemical oxidation [11]. In this way, the model allows the calculation of the efficiency of the electric energy from sun irradiance and the efficiency of the organic matter mineralization processes, which constitute useful parameters for the optimization of the PSEO process. As a result, an engineering approach to the problem is pursued so that an easy and useful model is obtained, with which a compromise between accuracy and simplicity is reached.

* Corresponding author. Tel.: +34 942 20 09 31; fax: +34 942 20 15 91.
E-mail address: alvarezge@unican.es (E. Alvarez-Guerra).

1385-8947/$ – see front matter © 2011 Elsevier B.V. All rights reserved.
doi:10.1016/j.cej.2011.02.043

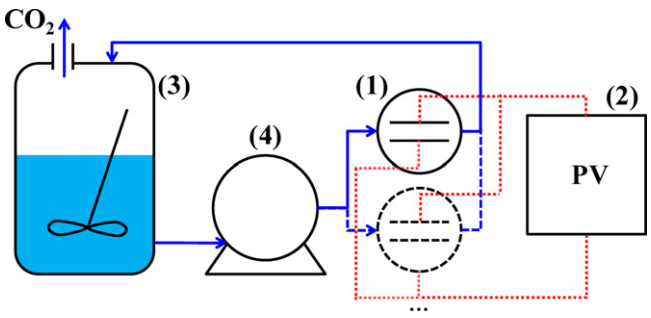

Fig. 1. Experimental set-up. (1) Electrochemical reactor(s). (2) Photovoltaic modules supply. (3) Refrigerated storage tank. (4) Centrifugal pump.

2. Materials and methods

Wastewaters studied in this work were both urban and synthetic. Urban wastewater was obtained from a primary decanter of the wastewater treatment plant of Aguilar de Campoo (Palencia, Spain). Synthetic solutions containing lignosulfonate or glucose were prepared. Sodium sulfate was added as supporting electrolyte of synthetic solutions, since the amount of lignosulfonate and glucose added gives the effluent relatively very low values of conductivity. However, the urban wastewater already has enough conductivity so supporting electrolyte is not necessary. The lignosulfonate used was commercial Borrebond 55S calcium–magnesium lignosulfonate coming from *Eucalyptus globules* (sulfite process) produced by Lignotech Iberica S.A. (Spain). Glucose and sodium sulfate were provided by Panreac Química S.A.U., whereas ultrapure water from Milli-Q was employed to prepare the synthetic solutions.

Fig. 1 shows the general diagram of the PSEO process analyzed in this work. Experiments were carried out at different scales, both lab and pilot plant scales:

2.1. Lab-scale experimental set-up

At lab-scale experiments, the electrochemical reactor consists of a single compartment flow DiaCell® Type 106: 02-06 (manufactured by Adamant Technologies SA). Electrodes are based on conductive thin-films of boron-doped diamond supported on a silicon substrate. Each compartment has an anode and a cathode of 70 cm^2 separated by an interelectrode gap of 1 mm. In these experiments, which were carried out in batch mode, the volume of wastewater treated was 2 L and it was pumped continuously to the electrochemical reactor so that the flow through the compartment was 300 $L\,h^{-1}$.

Regarding the electric energy generation by photovoltaic solar energy, up to 4 monocrystalline photovoltaic modules (SunTech STP 160) were directly connected to the electrochemical reactor (located on the roof of ETSIIyT, University of Cantabria, Santander, Spain, with a tilt at 38° and south orientation of 20° west). On the other hand, experiments focused on kinetic analysis were carried out at galvanostatic mode by using an Agilent power supply A6554.

2.2. Pilot plant-scale experimental set-up

Each DiaCell® 108.1001 electrochemical reactor contains 10 compartments, with BDD anodes and stainless steel cathodes. Regarding other characteristics, they are identical to the lab-scale electrochemical reactor. Consequently, as 5 reactors were employed in parallel configuration, the total anodic area of the pilot plant was 0.35 m^2. At this scale, 100 L were treated in batch experiments and the flow through each compartment was 360 $L\,h^{-1}$. All the experiments were carried out at galvanostatic mode with a Microswitch NGIP 750-16 rectifier (Micronics Systems).

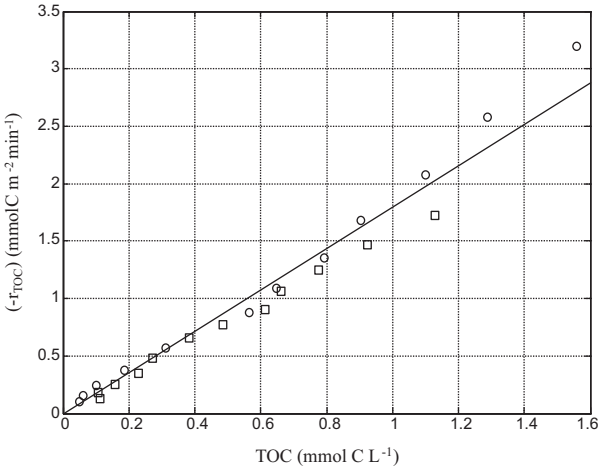

Fig. 2. Experimental reaction rates, $(-r_{TOC})$, vs. TOC of experiments carried out with urban wastewaters. (○) UWW-L-1; (□) UWW-L-2; (–) fitting curve of all the experiments.

2.3. Analytical procedure

Total organic carbon (TOC) was monitored during the experiments by means of a Shimadzu TOC-V CPH with ASI-V, operating with synthetic air from Air Liquide S.A., Spain (pressure: 200 kPa; flowrate: 150 $mL\,min^{-1}$). A Hach HQ40d unit (Hach Lange) was used to measure the pH and conductivity of the wastewater. The current intensity, voltage and electric power applied to the system formed by the electrochemical reactor and connecting wires were continuously recorded using a Fluke 345 unit (Fluke). A SunReader unit (SunTechnics Conergy Group) gave measurements of solar irradiance every 15 min.

3. Results and discussion

3.1. Organic matter mineralization process

Table 1 shows the characteristics of the set of experiments of this work to study the total organic carbon (TOC) removal. As can be seen from Table 1, different types of effluents in both lab and pilot scales have been analyzed in order to determine the influence of the pollutant. Regarding experimental conditions, the effect of the current density applied, i, and the initial TOC of the effluent, TOC_0, have been considered.

The reaction rate of the organic matter mineralization process, $(-r_{TOC})$, is referred to the anodic area, A_a, as extensive magnitude, since this surface or the very adjacent fluid layer are the regions in which this reaction takes place [16,17]:

$$(-r_{TOC}) = -\frac{1}{A_a}\frac{dn_{TOC}}{dt} = -\frac{V_s}{A_a}\frac{dTOC}{dt} \quad (1)$$

where V_s is the effluent volume treated in the electrochemical system and n_{TOC} is the number of carbon moles contained in V_s. The reaction rates $(-r_{TOC})$ were obtained from the experimental TOC-time data.

Figs. 2–4 show the reaction rate $(-r_{TOC})$ vs. the TOC of the effluent. The reaction rate gives values up to 3.2, 91 and 44 $mmol\,C\,m^{-2}\,min^{-1}$, whereas TOC reaches 1.6, 47 and 33 $mmol\,C\,L^{-1}$, for the series of experiments carried out with urban wastewater, glucose and lignosulfonate, respectively. As can be seen for all the experiments, a linear relationship between $(-r_{TOC})$ and TOC is observed, and a first order kinetics with respect to the

Table 1
Characteristics of the set of experiments analyzed to describe the total organic carbon (TOC) degradation process.

Experiment code	Effluent	Scale	i (mA cm^{-2})	Initial TOC (mmol C L^{-1})	Na_2SO_4 (mg L^{-1})
UWW-L-1	Urban wastewater	Lab	30	1.56	0
UWW-L-2	Urban wastewater	Lab	15	1.13	0
G-L-1	Synthetic wastewater (glucose)	Lab	10	0.90	2500
G-L-2	Synthetic wastewater (glucose)	Lab	10	0.53	2500
G-L-3	Synthetic wastewater (glucose)	Lab	15	0.92	2500
G-L-4	Synthetic wastewater (glucose)	Lab	30	12.4	2500
G-L-5	Synthetic wastewater (glucose)	Lab	60	1.64	2500
G-P-1	Synthetic wastewater (glucose)	Pilot	30	14.9	2500
G-P-2	Synthetic wastewater (glucose)	Pilot	60	47.1	2500
LS-L-1	Synthetic wastewater (lignosulfonate)	Lab	60	8.82	2500
LS-L-2	Synthetic wastewater (lignosulfonate)	Lab	60	30.9	2500
LS-P-1	Synthetic wastewater (lignosulfonate)	Pilot	15	11.8	2500
LS-P-2	Synthetic wastewater (lignosulfonate)	Pilot	30	12.2	2500
LS-P-3	Synthetic wastewater (lignosulfonate)	Pilot	60	33.2	2500

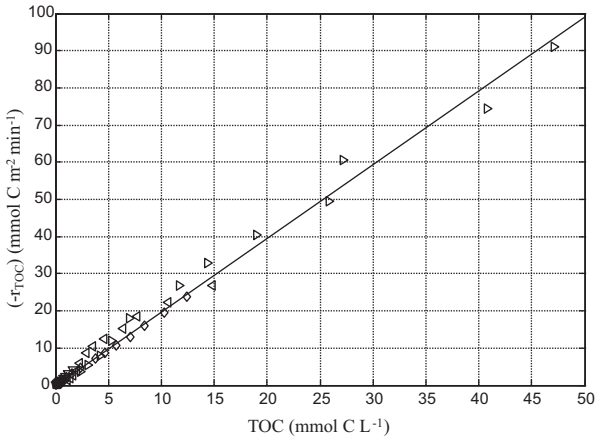

Fig. 3. Experimental reaction rates, $(-r_{TOC})$, vs. TOC of experiments carried out with glucose. (○) G-L-1; (□) G-L-2; (+) G-L-3; (◊) G-L-4; (▽) G-L-5; (◁) G-P-1; (▷) G-P-2; (–) fitting curve of all the experiments.

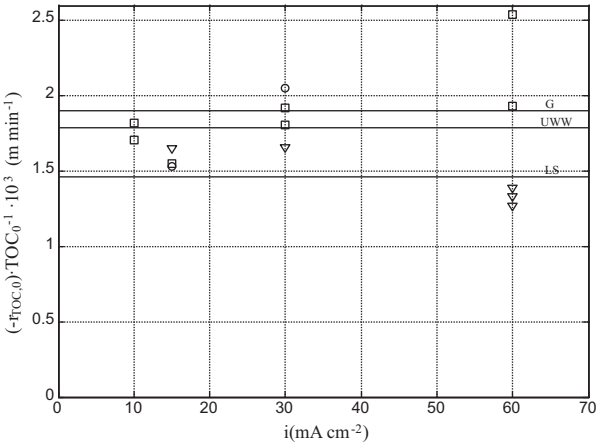

Fig. 5. Initial rate analysis. (○) UWW (urban wastewater) series of experiments; (□) G (glucose) series of experiments; (▽) LS (lignosulfonate) series of experiments; (–) mean value of the series whose code is written above the line.

TOC concentration is concluded for all the experiments. On the other hand, the reaction rate is independent of the current density, i, because experiments were carried out at different i values and no relevant trend was detected: data from experiments with different values of i give similar $(-r_{TOC})$ for the same TOC values.

On the other hand, the independence of $(-r_{TOC})$ from current density can be observed clearly in Fig. 5, where initial conditions $(-r_{TOC,0}) \cdot TOC_0^{-1}$ vs. i are shown. Points of the same type of effluent have similar values of $(-r_{TOC,0}) \cdot TOC_0^{-1}$ (which means the same rate constant), despite their very different values of i. In this way, data of each type of effluent appear around a mean value for all the range of current densities.

Consequently, the rate equation for the mineralization process that describes the experimental behavior is:

$$(-r_{TOC}) = k \cdot TOC \quad (2)$$

where k is the rate constant. This kinetic equation describes the process in the researched range of variables.

Table 2 shows the value of the rate constant for each series of experiments (those which treat the same type of effluent).

The value of k remains constant for each experiment, since no deviation is detected at relatively low or high TOC values: k does not vary during each experiment due to the TOC reduction, describing with the same value all the mineralization process. Moreover, it can be concluded that results are not affected by the scale (laboratory and pilot plant) when the ratio A_a/V_s is remained constant (in this case, 3.5 m^{-1}) since the mineralization rates obtained at each scale for the same effluent are practically identical. This agrees

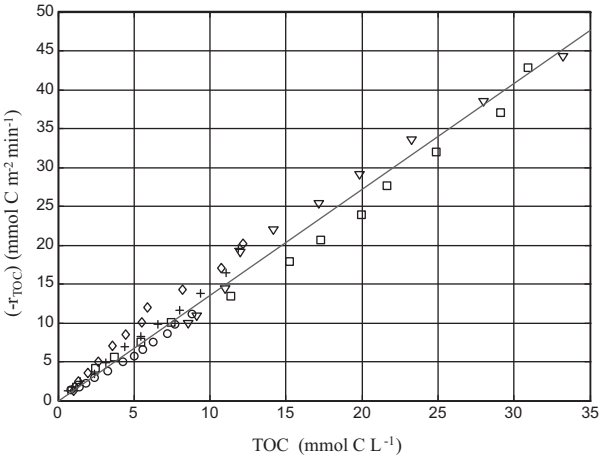

Fig. 4. Experimental reaction rates, $(-r_{TOC})$, vs. TOC of experiments carried out with lignosulfonate. (○) LS-L-1; (□) LS-L-2; (+) LS-P-1; (◊) LS-P-2; (▽) LS-P-3; (–) fitting curve of all the experiments.

Table 2
First order kinetic constant, k, for each series of experiments (confidence level at 95%).

Exp. series	$k \times 10^3$ (m min^{-1})	R^2
UWW	1.80 ± 0.09	0.968
Glucose	1.98 ± 0.04	0.997
LS	1.36 ± 0.04	0.976

Table 3
Characteristics of the set of experiments analyzed to describe the electric energy generation with photovoltaic modules directly connected to the electrochemical reactor.

Experiment code	No. of PV modules	Weather	Supporting electrolyte (Na_2SO_4 g L^{-1})
Exp. 1	2	Sunny	2.5
Exp. 2	4	Sunny	2.5
Exp. 3	2	Sunny/cloudy	2.5
Exp. 4	1	Sunny/cloudy	0.3

well with the idea that results and conclusions obtained at lab-scale are transferable to the scale-up of these electrode-based systems [18,19].

However, some variability in the mineralization rate by means of the value of k is observed among experiments of the same series. These differences can be explained in terms of sensitivity of the experimental results to the state of the electrode, what can have an influence on its activity, effective area, etc., as factors which affect the mineralization rate. Sensitivity is especially important in initial rate data of Fig. 5, since each experiment is represented by a single point, instead of a series like in Figs. 2–4.

Regarding the effluent nature, lignosulfonate mineralization rates are described by means of a rate constant significantly lower ($k = 1.36 \times 10^{-3}$ m min^{-1}) than those observed in the rest of experiments. It can be justified considering that lignosulfonate is a biorefractory, high-molecular weight pollutant [20]. On the other hand, glucose, an easily oxidative organic compound [21], presents the highest average value of the constant rate ($k = 1.98 \times 10^{-3}$ m min^{-1}). In fact, urban wastewater presents an intermediate mineralization rate ($k = 1.80 \times 10^{-3}$ m min^{-1}), since it is constituted by a mixing of many different organic compounds. Fig. 5 also shows the same trend of the mineralization rate with effluent nature: the mean values obtained for each series of experiments are very close to the rate constant values shown in Table 2. High conversions are reached for all the effluents considered, which implies that electrochemical oxidation with BDD electrodes is able to mineralize a large number of organic compounds [4].

3.2. Solar photovoltaic electro-oxidation process: energy balance, analysis and modeling

Once the kinetics of the mineralization process is well-known, an energy balance has to be applied in order to describe how the solar energy is converted into electric energy and then, how the latter is used in the electrochemical reactions. The model pursues to describe the TOC of the effluent (output) as a function of solar irradiance and the initial TOC (inputs). Moreover, two efficiencies have to be defined from model equations to give measures of the process performance and, in this way, to achieve the optimum design of the system.

Regarding the electric energy generation, a set of experiments were carried out to analyze the performance of photovoltaic (PV) modules when they are connected to the electrochemical reactor in different operating conditions, which are summarized in Table 3.

Fig. 6 shows the relationship between the electric current intensity, I, and the solar incident power in the whole set of PV modules. This solar incident power is given by $NA_{PV}G$, where N is the number of PV modules; A_{PV} is the area of each PV module and G is the solar irradiance. A linear dependence between I and $NA_{PV}G$ is shown, so data can be adjusted to a linear relationship with zero interception ($R^2 = 0.994$):

$$I = 4.43 \times 10^{-3} NA_{PV}G \quad (3)$$

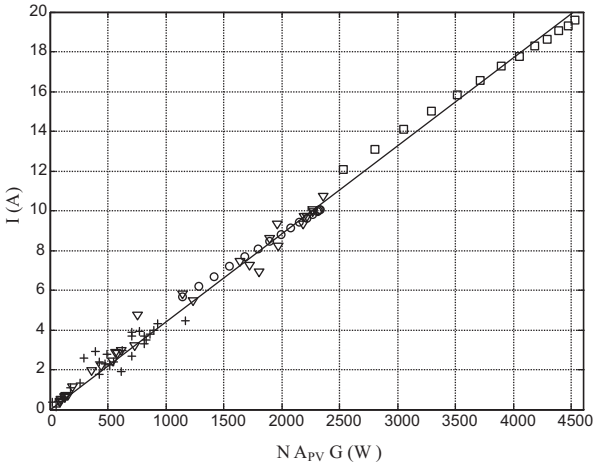

Fig. 6. Electric current, I, generated by the PV modules at different solar irradiances, G. (○) Exp. 1; (□) Exp. 2; (▽) Exp. 3; (+) Exp. 4; (–) linear fitting of all the experiments.

Some data from experiments 3 and especially 4 correspond to high patchy cloud periods. Consequently, this fact makes that these points appear in Fig. 6 far from the line described by Eq. (3). The I–$NA_{PV}G$ linear relationship implies these main assumptions introduced in the PV performance:

- Modules always operate at the region in which the current is near short-circuit current, I_{sc}, in order to supply as many electrons as possible to the cell.
- In this region, which includes a wide range of voltages, the current is considered approximately constant with voltage [13]. In more complex models, such as 1 diode models, this fact is equivalent to the shunt resistance of the solar cells, R_{sh}, is infinite [22,23].
- Temperature effect is not considered in the operating conditions, since in this work, modules are installed in a region with mild climate.
- Second order effects (non-linearity due to low resistance, effects of wind, etc. [24]) are assumed negligible.

Under these assumptions, the slope of the I–$NA_{PV}G$ relationship, α, can be correlated to I_{sc}, A_{PV}, and the solar irradiances at reference conditions, G_{ref}, as follows:

$$\alpha = \frac{I_{sc}}{A_{PV}G_{ref}} \quad (4)$$

For the experiments carried out at laboratory scale, $\alpha = 4.44 \times 10^{-3}$ A W^{-1}, which fits the value that was obtained adjusting the I–$NA_{PV}G$ experimental data (see Fig. 6).

However, the power supplied by the PV modules, P, not only depends on the electric current, but also on the voltage generated at the terminals of the load connected to the mentioned modules. In this way, Fig. 7 represents voltage, V, vs. current density, i, in order to observe the relationship between them. V varies between 2.5 and 14.8 V, whereas i shows values between 1 and 280 mA cm^{-2}. Current density is chosen instead of electric current to achieve that the electrochemical reactor configuration does not affect to the analysis of the voltage. For high values of i, Fig. 7 states that V increases linearly with i. This linear relationship is represented by ohmic resistances. Among these resistances, only the effluent resistance is usually considered [25,26]. Nevertheless, for low values of i, the linear relationship cannot describe the experimental data, since V decreases faster with current density until it reaches an ordinate origin significantly lower than the one of the straight line constituted by data at high i. This non-linear region of the V–i curve can be explained in terms of the equilibrium potentials and overpoten-

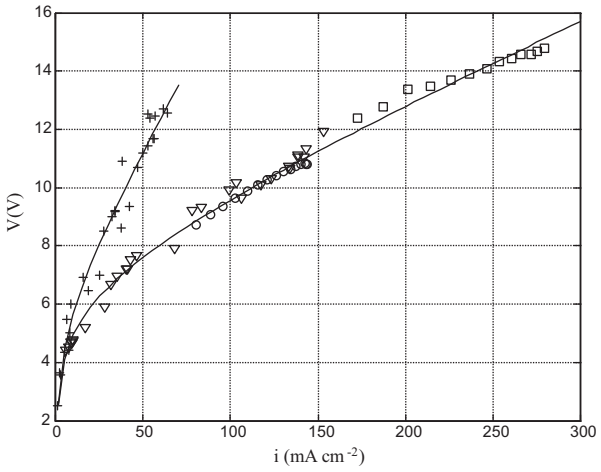

Fig. 7. Voltage, V, vs. current density, i, generated by the PV modules. (◯) Exp. 1; (□) Exp. 2; (▽) Exp. 3; (+) Exp. 4; (–) adjusting equation line for different values of conductivity.

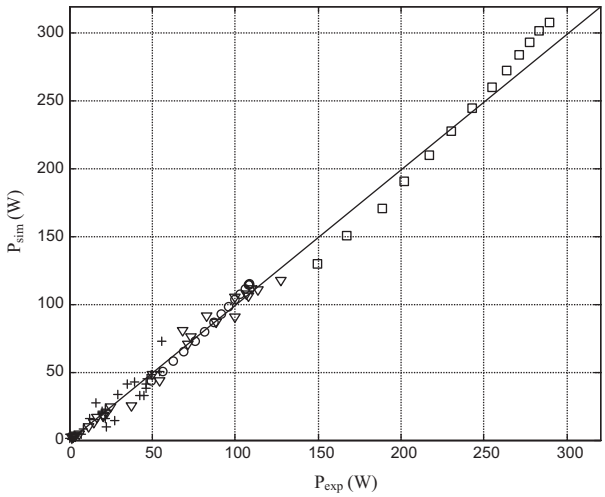

Fig. 8. Parity chart of the theoretical power predicted by the model, P_{sim}, vs. the experimental generated power, P_{exp}. (◯) Exp. 1; (□) Exp. 2; (▽) Exp. 3; (+) Exp. 4; (–) line which represents equality between simulated and experimental values.

tials of the electrodes. Experimental V–i data have been adjusted to Eq. (5) to describe the trend observed [26]:

$$V = a + b \cdot \log i + c \cdot i \tag{5}$$

where a, b and c are adjusting coefficients. The first two terms of Eq. (5), which include a and b, are associated to the equilibrium potentials and overpotentials of the electrodes. On the other hand, c introduces the linear relationship between V and i, so it is related to effluent resistance, which is a function of the conductivity, λ.

The values of the adjusting coefficients when V and i are expressed in V and mA cm^{-2}, respectively, are: $a = 2.28 \pm 0.35$; $b = 2.41 \pm 0.30$; $c = 0.0248 \pm 0.0023$ – for experiments 1–3 – and $c = 0.0969 \pm 0.0062$ – for experiment 4 – ($R^2 = 0.986$ and confidence level at 95%). Different values of c are explained because of the different conductivity at which experiments were carried out: in experiments 1–3, 2.5 g Na_2SO_4 L^{-1} were used as supporting electrolyte ($\lambda = 3.6$ mS cm^{-1}), whereas only 0.3 g Na_2SO_4 L^{-1} were added to the effluent in experiment 4 ($\lambda = 1.0$ mS cm^{-1}). In this way, as c (ohmic resistance) is inversely proportional to conductivity, the ratio $c_{exp.\,4}/c_{exp.\,1-3}$ (3.9) is similar to the ratio $\lambda_{exp.\,1-3}/\lambda_{exp.\,4}$ (3.6).

Eqs. (2)–(5) constitute the PSEO model, which is required to size the main equipments of the process: the electrochemical reactor and the PV modules. Further research on this technology related to the equipment design and investment cost is ongoing. Once the PSEO process has been described, two efficiencies are introduced in order to measure its performance:

- Energy conversion efficiency, η_e, which expresses the solar energy converted into electric energy by the modules at each instant.
- Current efficiency, η_c, which measures the fraction of the current generated that is employed in the desired reactions of mineralization of organic compounds.

In order to calculate η_e, it is necessary to obtain the power generated by PV modules, P, which is calculated as:

$$P = IV \tag{6}$$

Fig. 8 represents the parity chart of the theoretical power predicted by the model, P_{sim}, vs. the experimental generated power, P_{exp}. As can be seen, all points are near the line that represents the agreement between simulated and experimental data, so with this simple model the behavior of the photovoltaic modules can be described, reaching a compromise between accuracy and complexity. As a result, η_e is defined according to the following expression:

$$\eta_e = \frac{P}{NA_{PV}G} \tag{7}$$

Considering Eqs. (3)–(6) and that I is related with i by means of the anodic area, A_a, P is replaced in Eq. (7) and it is obtained:

$$\eta_e = \alpha \left[a + b \log \left(\frac{\alpha N A_{PV} G}{A_a} \right) + c \left(\frac{\alpha N A_{PV} G}{A_a} \right) \right] \tag{8}$$

Therefore, η_e is a function of the model parameters related to electric energy generation (α, a, b and c), the equipment parameters (N, A_{PV} and A_a) and the solar irradiance (G). The dependence of η_e on G implies that the efficiency of the PV modules cannot be considered as constant during experiments. It should be noted that other efficiencies can be defined to describe PV modules behavior, like the efficiency of solar modules under standard test conditions, η_{STC}, or the performance ratio, PR. η_{STC} is the ratio of the module to the radiative power falling on it (which is only function of module parameters), and PR is the ratio of the actual electric energy generated to the energy production of an ideal, loss-less PV plant with 25 °C cell temperature and the same solar irradiation [27,28].

Respecting the organic matter mineralization process, the kinetics obtained in Section 3.1 allows the calculation of the output TOC, for a given input TOC_0. Furthermore, it is also necessary to know the volume of the effluent, V_s, and the treatment time, t, for systems operating at discontinuous mode, or the space-time, τ, for continuous processes. Moreover, in order to compare the mineralization rate, $(-r_{max})$ is defined. $(-r_{max})$ represents the maximum rate that can be achieved with a given current density and it corresponds to the case in which all the electrons supplied to the electrochemical reactor are involved in the desired reaction of mineralization of organic matter [29,30]:

$$(-r_{max}) = \frac{i}{nF} \tag{9}$$

where n is the number of electrons involved in the organic matter mineralization (4 mol e$^-$ mol C^{-1}) and F is the Faraday constant (96,485 C mol^{-1}).

The current efficiency, η_c, can be defined as a ratio of rates as follows:

$$\eta_c = \frac{(-r_{TOC})}{(-r_{max})} \tag{10}$$

As a consequence, substituting Eqs. (2) and (9) into Eq. (10), it is concluded that the model developed in the present work predicts

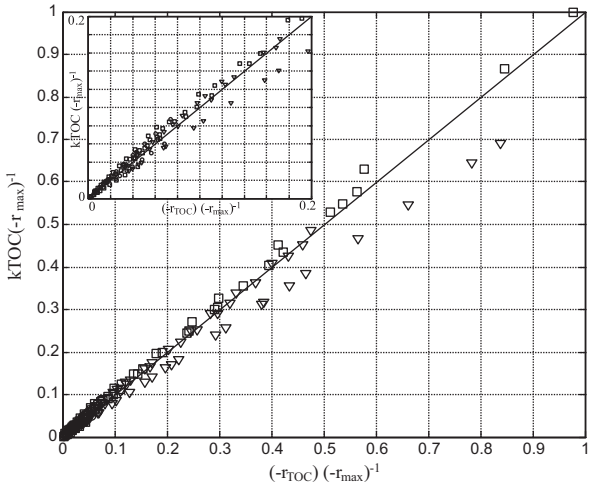

Fig. 9. Parity chart of the current efficiency predicted by the model, $k\mathrm{TOC}\cdot(-r_{\max})^{-1}$ vs. the experimental current efficiency, $(-r_{\mathrm{TOC}})\cdot(-r_{\max})^{-1}$. (○) UWW (urban wastewater) series of experiment; (□) G (glucose) series of experiment; (▽) LS (lignosulfonate) series of experiment; (–) line which represents equality between simulated and experimental values.

a current efficiency for the conditions of mass-transport control equals the following expression:

$$\eta_{\mathrm{c}} = \frac{nFk\mathrm{TOC}}{i} \tag{11}$$

A fraction of the electrical energy is involved in undesired secondary reactions, such as oxygen evolution, since η_{c} is lower than unity [31]. In the experiments analyzed, observed mineralization rates, $(-r_{\mathrm{TOC}})$, do not reach $(-r_{\max})$. In this way, if the current density is increased, as $(-r_{\mathrm{TOC}})$ does not vary with this variable, η_{c} decreases in the same proportion (Eq. (11)). On the other hand, for a given current density, the higher TOC, the higher η_{c}, due to the linear relationship between TOC and η_{c}.

Fig. 9 shows the current efficiency predicted by the model (Eq. (11)) vs. the experimental efficiency obtained as $(-r_{\mathrm{TOC}})\cdot(-r_{\max})^{-1}$. The vast majority of points are very close to the line which represents equality between simulated and experimental values. This implies the accuracy of the organic matter mineralization model. Only a few points corresponding to experiment LS-P-1 present a significant deviation, despite the fact that this should be interpreted in terms of the variability of the mineralization rate as previously stated.

4. Conclusions

The photovoltaic solar electrochemical oxidation (PSEO) process can be described with both accuracy and simplicity by means of the model developed in this work, considering a process engineering approach. This model has been successfully applied to different types of effluents and laboratory and pilot plant scales. The organic matter mineralization rate is independent from current density and it presents a first order kinetics with respect to TOC. Electric energy generation in photovoltaic modules can be described by the linear relationship between current and solar irradiance, since the modules operated in the region in which current does not depend on voltage. Moreover, the model makes it possible to define two efficiencies: energy conversion efficiency, η_{e}, representing the solar energy converted into electric energy by the PV modules; and current efficiency, η_{c}, describing the ratio of the observed mineralization rate to the maximum rate. These efficiencies will allow a design optimization depending on the process variables.

Acknowledgements

The authors gratefully acknowledge the financial support of the Ministry of Science and Technology of Spain through the project CTM2006-00317 and the project CENIT Sostaqua.

References

[1] C.A. Martínez-Huitle, E. Brillas, Decontamination of wastewater containing synthetic organic dyes by electrochemical methods: a general review, Appl. Catal. B 87 (2009) 105–145.
[2] Á. Anglada, A. Urtiaga, I. Ortiz, Contributions of electrochemical oxidation to waste-water treatment: fundamentals and review of applications, J. Chem. Technol. Biotechnol. 84 (2009) 1747–1755.
[3] F. Montilla, P.A. Michaud, E. Morallón, J.L. Vázquez, Ch. Comninellis, Electrochemical oxidation of benzoic acid at boron-doped diamond electrodes, Electrochim. Acta 47 (2002) 3509–3513.
[4] M. Panizza, G. Cerisola, Application of diamond electrodes to electrochemical processes, Electrochim. Acta 51 (2005) 191–199.
[5] M.A. Rodrigo, P. Cañizares, A. Sánchez-Carretero, C. Sáez, Use of conductive-diamond electrochemical oxidation for wastewater treatment, Catal. Today 151 (2010) 173–177.
[6] Á. Anglada, A.M. Urtiaga, I. Ortiz, Laboratory and pilot plant scale study on the electrochemical oxidation of landfill leachate, J. Hazard. Mater. 181 (2010) 729–735.
[7] F.E. Hancock, Catalytic strategies for industrial water re-use, Catal. Today 53 (1999) 3–9.
[8] M. Panizza, P.A. Michaud, G. Cerisola, C. Comninellis, Electrochemical treatment of wastewaters containing organic pollutants on boron-doped diamond electrodes: prediction of specific energy consumption and required electrode area, Electrochem. Commun. 3 (2001) 336–339.
[9] A. Anglada, D. Ortiz, A.M. Urtiaga, I. Ortiz, Electrochemical oxidation of landfill leachates at pilot scale: evaluation of energy needs, Water Sci. Technol. 61 (2010) 2211–2217.
[10] H. Park, C.D. Vecitis, M.R. Hoffmann, Solar-powered electrochemical oxidation of organic compounds coupled with the cathodic production of molecular hydrogen, J. Phys. Chem. A 112 (2008) 7616–7626.
[11] A. Dominguez-Ramos, R. Aldaco, A. Irabien, Photovoltaic solar electrochemical oxidation (PSEO) for treatment of lignosulfonate wastewater, J. Chem. Technol. Biotechnol. 85 (2010) 821–830.
[12] T. Ochiai, K. Nakata, T. Murakami, A. Fujishima, Y. Yao, D.A. Tryk, Y. Kubota, Development of solar-driven electrochemical and photocatalytic water treatment system using a boron-doped diamond electrode and TiO_2 photocatalyst, Water Res. 44 (2010) 904–910.
[13] D. Valero, J.M. Ortiz, E. Expósito, V. Montiel, A. Aldaz, Electrochemical wastewater treatment directly powered by photovoltaic panels: electrooxidation of a dye-containing wastewater, Environ. Sci. Technol. 44 (2010) 5182–5187.
[14] M. Thomson, D. Infield, A photovoltaic-powered seawater reverse-osmosis system without batteries, Desalination 153 (2003) 1–8.
[15] M. Thomson, D. Infield, Laboratory demonstration of a photovoltaic-powered seawater reverse-osmosis system without batteries, Desalination 183 (2005) 105–111.
[16] A. Kapalka, G. Fóti, C. Comninellis, Kinetic modelling of the electrochemical mineralization of organic pollutants for wastewater treatment, J. Appl. Electrochem. 38 (2008) 7–16.
[17] C.R. Costa, F. Montilla, E. Morallón, P. Olivi, Electrochemical oxidation of synthetic tannery wastewater in chloride-free aqueous media, J. Hazard. Mater. 180 (2010) 429–435.
[18] I. Tröster, M. Fryda, D. Herrmann, L. Schäfer, W. Hänni, A. Perret, M. Blaschke, A. Kraft, M. Stadelmann, Electrochemical advanced oxidation process for water treatment using DiaChem® electrodes, Diamond Relat. Mater. 11 (2002) 640–645.
[19] X. Zhu, J. Ni, J. Wei, X. Xing, H. Li, Y. Jiang, Scale-up of BDD anode system for electrochemical oxidation of phenol simulated wastewater in continuous mode, J. Hazard. Mater. 184 (2010) 493–498.
[20] A. Dominguez-Ramos, R. Aldaco, A. Irabien, Electrochemical oxidation of lignosulfonate: total organic carbon oxidation kinetics, Ind. Eng. Chem. Res. 47 (2008) 9848–9853.
[21] A.M. Polcaro, M. Mascia, S. Palmas, A. Vacca, Electrochemical oxidation of phenolic and other organic compounds at boron doped diamond electrodes for wastewater treatment: effect of mass transfer, Ann. Chim-Rome 93 (2003) 967–976.
[22] J.M. Ortiz, E. Expósito, F. Gallud, V. García-García, V. Montiel, A. Aldaz, Photovoltaic electrodialysis system for brackish water desalination: modeling of global process, J. Membr. Sci. 274 (2006) 138–149.
[23] A.N. Celik, N. Acikgoz, Modelling and experimental verification of the operating current of mono-crystalline photovoltaic modules using four- and five-parameter models, Appl. Energ. 84 (2007) 1–15.
[24] E. Lorenzo, Electricidad solar fotovoltaica. Volumen II. Radiación solar y dispositivos fotovoltaicos (Photovoltaic Solar Energy. Volume II. Solar radiation and photovoltaic devices), PROGENSA, Seville, Spain, 2006.
[25] C.G. Alfafara, T. Kawamori, N. Nomura, M. Kiuchi, M. Matsumura, Electrolytic removal of ammonia from brine wastewater: scale-up, operation and pilot-scale evaluation, J. Chem. Technol. Biotechnol. 79 (2004) 291–298.

[26] G. Chen, Electrochemical technologies in wastewater treatment, Sep. Purif. Technol. 38 (2004) 11–41.
[27] A. Luque, S. Hegedus, Handbook of Photovoltaic Science and Engineering, John Wiley & Sons, Chichester, England, 2003.
[28] A. Goetzberger, V.U. Hoffmann, Photovoltaic Solar Energy Generation, Springer, Berlin, Germany, 2005.
[29] P. Cañizares, J. Lobato, R. Paz, M.A. Rodrigo, C. Sáez, Electrochemical oxidation of phenolic wastes with boron-doped diamond anodes, Water Res. 39 (2005) 2687–2703.
[30] P. Cañizares, L. Martínez, R. Paz, C. Sáez, J. Lobato, M.A. Rodrigo, Treatment of Fenton-refractory olive oil mill wastes by electrochemical oxidation with boron-doped diamond anodes, J. Chem. Technol. Biotechnol. 81 (2006) 1331–1337.
[31] M. Panizza, A. Kapalka, Ch. Comninellis, Oxidation of organic pollutants on BDD anodes using modulated current electrolysis, Electrochim. Acta 53 (2008) 2289–2295.